

Digital resonance tuning of high- Q/V_m silicon photonic crystal nanocavities by atomic layer deposition

Xiaodong Yang^{1,2}, Charlton J. Chen¹, Chad A. Husko, and Chee Wei Wong²
Optical Nanostructures Laboratory, Columbia University, New York, NY 10027

We propose and demonstrate for the first time the digital tuning of high- Q/V_m photonic crystal resonances using a self-limiting atomic layer deposition technique. Control of resonances in discrete steps of 122 ± 18 pm per hafnium oxide atomic layer is achieved through this post-fabrication process, nearly linear over a full 17 nm tuning range. The cavity Q is maintained in this perturbative process, and can reach up to its initial values of 49,000 or more. Our results are highly controllable, applicable to many material systems, and particularly critical to matching resonances and transitions involving mesoscopic optical cavities.

Two-dimensional photonic crystal (2D PhC) slabs confine light by Bragg reflection in-plane and total internal reflection in the third dimension. Introduction of point and line defects into 2D PhC slabs create localized resonant cavities and PhC waveguides respectively, with ab initio arbitrary dispersion control. Such defect cavities in high-index contrast materials possess strong confinement with subwavelength modal volumes (V_m) at $\sim (\lambda/n)^3$, corresponding to high field intensities per photon for increased nonlinear interaction. Moreover, photonic crystal cavities with remarkable high quality factors (Q) [1, 2] have been achieved recently, now permitting nanosecond photon lifetimes for enhanced light-matter interactions. The strong localization and long photon lifetimes in these high- Q/V_m photonic crystal nanocavities point to enhanced nonlinear optical

¹ These authors contributed equally to this work.

² Electronic mail: xy2103@columbia.edu, cww2104@columbia.edu

physics, such as optical bistability [3-5], Raman lasing [6, 7] and cavity quantum electrodynamics [8] in silicon photonics.

These applications require precise control of cavity modes to achieve maximum spectral overlap between cavity modes and gain material for best device performance. The cavity resonances can be widely tuned by adjusting the lattice constant a and the hole radius r of photonic crystal slabs through fabrication. However the position of mode resonance is highly sensitive to the fabrication process. Active tuning using thermal (with associated phonon broadening of quantum dots) [9] or piezoelectric effects [10] can be employed. A passive post-fabrication tuning mechanism is particularly demanded, without external input power, to precisely align the designed resonant wavelengths. Specifically, wet chemical digital etching techniques [11] were recently developed for GaAs photonic crystal nanocavities, where the controlled blue shift of the cavity resonance was around 2-3 nm/cycle. Additionally, condensation of Xe [12] or self-assembled monolayers (such as a 2-nm polypeptide monolayer) can be used [13], where a 3-5 nm cavity red shift per monolayer was observed for the latter. To achieve hundreds of picometer cavity resonance tuning, thin films below one nanometer is needed to be etched or deposited.

Atomic layer deposition (ALD) is widely used for gate dielectric and capacitance memory applications due to its precise thickness control and highly conformal film. Several metal oxides such as aluminum oxide (Al_2O_3), hafnium oxide (HfO_2), and titanium dioxide (TiO_2) have been used in low temperature ALD thin film growth. All these materials have been widely used in optical coating applications with a relatively high refractive index (refractive index at 1.55 μm , $n = 1.88$ for HfO_2 [14], $n = 1.57$ for Al_2O_3 [15], and $n = 2.18$ for TiO_2 [16]) and low absorption over a wide spectral range, extending from the near-ultraviolet to the mid-infrared (direct band gap is 5.41 eV for HfO_2). Recently, ALD has become a promising tool for the fabrication of high quality three-dimensional photonic crystals from inorganic and organic templates with TiO_2 [17] and Al_2O_3 [18]. Photonic band structure tuning in a 2D periodic lattice was also demonstrated, with 12% tuning range and 0.005% precision based on a deposition rate of 0.51 \AA TiO_2 per ALD cycle [19].

In this Letter, we report the post-fabrication digital resonant wavelength tuning of high- Q/V_m silicon photonic crystal nanocavities using self-limiting atomic layer deposition of HfO_2 . The vertical radiation from the top of nanocavities was collected to analyze the mode resonances after each conformal coating step with slightly decreased r/a and increased t/a ratios in air-bridged photonic crystal slabs. The results demonstrate wide tuning range and precise fine control of cavity resonances while preserving high quality factors. The observed deposition rate is around 0.93 \AA HfO_2 per ALD cycle, which leads to the red shift of resonant wavelength with precision of $122 \pm 18 \text{ pm}$ for a resonant wavelength $\sim 1.55 \text{ }\mu\text{m}$. Total resonant wavelength tuning range is around 17 nm and only limited by current seven deposition steps used.

The structure investigated is an air-bridged triangular lattice photonic crystal slab with silicon membrane thickness of 190 nm ($t/a = 0.4524$) and air holes radii of 90 nm ($r/a = 0.2143$), where the lattice period $a = 420 \text{ nm}$. High- Q/V_m nanocavities with five linearly aligned missing air holes ($L5$) are side coupled with photonic crystal waveguides, as shown in Figure 1(a). The shift S_l of two air-holes at cavity edge is $0.02a$, $0.06a$ and $0.10a$, respectively, for three different $L5$ nanocavities studied, in order to tune the radiation mode pattern for increasing the Q factors. The waveguide-to-cavity separation is five layers of holes. The devices were initially patterned with deep UV lithography at the Institute of Microelectronics in Singapore, and subsequently etched with a $\text{SF}_6/\text{C}_4\text{F}_8$ -based inductively coupled plasma (ICP) into a silicon-on-insulator substrate. Next, optical lithography with AZ4620 photoresist was used to open a window in photonic crystal region, and 10 minutes HF BOE (6:1) used to release the air-bridged structures. Samples were then cleaned using Piranha ($\text{H}_2\text{SO}_4:\text{H}_2\text{O}_2$ 3:1) solution for 5 minutes followed by HF BOE (6:1) solution dip for 30 seconds and deionized water rinse. Hot methanol was used as the final rinsing liquid to prevent stiction with the lower surface tension of methanol compared to water. This procedure results in $\sim 6 \text{ \AA}$ of (O-H)-terminated silicon oxide on the surface of silicon air-bridged photonic crystal slabs [20]. All samples were exposed to UV generated ozone for 10 minutes to restore the hydrophilic character of surface immediately prior to HfO_2 deposition. Figure 1(a) shows the top-view scanning electron microscopy (SEM) image of air-bridged $L5$ cavity with $S_l = 0.02a$ before ALD. Figure 1(e) shows the electric field E_y of the resonance mode mid-

slab from 3D finite-difference time-domain simulations, calculated using a freely available software package with subpixel smoothing for increased accuracy [21].

Thin films of amorphous HfO_2 are deposited conformally on silicon air-bridged photonic crystal slabs by means of ALD at 150°C . Films were deposited using tetrakis(diethylamido)hafnium (IV) $[\text{Hf}(\text{DEA})_4]$ and water (H_2O) vapor in alternating pulses with N_2 purge of the reaction chamber between pulses. Each deposition step includes 20 ALD cycles, where each cycle consists of $\text{Hf}(\text{DEA})_4$ injection for 0.25 s, N_2 purge for 150 s, H_2O injection for 0.02 s, and N_2 purge for 200 s. The observed linear deposition rate is around 0.93 \AA per cycle, which is about a monolayer of hafnium oxide. We note that lower substrate temperature down to 90°C is possible with our machine, at the expense of slow deposition rates. Figure 1(b) shows the top-view SEM image of $L5$ cavity after seven deposition steps, with the same magnification as in Figure 1(a). Based on geometrical statistical analysis of high-resolution SEM images, the hole radius reduces from $92.84 \pm 1.56 \text{ nm}$ to $79.86 \pm 2.66 \text{ nm}$ [22]. Figure 1(c) and 1(d) are the angled-view SEM images of air-bridged photonic crystal slabs before ALD and after seven deposition steps, respectively. The surface is still smooth enough to support high- Q modes for $L5$ nanocavities after HfO_2 deposition. The thickness of photonic crystal slabs increases from 190 nm to 216 nm based on SEM estimates. These geometry changes agree well with the deposition schematic cross section of the sample morphology drawn in Figure 1(f).

With slightly decreased r/a and increased t/a ratios in air-bridged photonic crystal slabs, the photonic band gap will shift to lower frequencies. In addition to a frequency shift, the photonic bandgap also decreases from an 11.4% to a 9.7% gap with a deposition of HfO_2 , computed using a freely available software package [23]. This can be attributed to a lower-index contrast between the holes and the bulk dielectric. The resonant wavelength of $L5$ nanocavities will undergo a red shift.

For the measurement setup, a polarization controller and a lensed fiber are used to couple transverse-electric (TE) polarization light from tunable laser source (1480-1580 nm, wavelength accuracy 10 pm with 200 kHz linewidth) into the waveguide. A second lensed fiber collects the transmission from the waveguide output to check the total transmission loss of the whole system, which is around 24.8 dBm at wavelength of 1550 nm. The vertical radiation from the top of nanocavities collected by a 40X objective lens

(NA 0.65) and a 4X telescope was sent to the photodetector and lock-in amplifier to analyze the cavity resonances. In order to exclude optical nonlinear effects, low input power of 10 μW was coupled to the waveguide. Figure 2(a) plots the measured cavity resonances after each deposition step for $L5$ cavity with $S_I = 0.02a$. Figure 2(b) magnifies the resonance peak after the fourth deposition step. The quality factor Q is estimated from the full-width at half maximum and is $\sim 49,000$. From the 3D FDTD method, the Q factor and modal volume are calculated around 50,000 and ~ 0.98 cubic wavelengths $((\lambda/n)^3)$ respectively.

Figure 3(a) shows the tuned resonant wavelength scales linearly with the number of deposition steps for all three $L5$ cavities under investigation. Total resonant wavelength tuning range is around 17 nm with current seven deposition steps. With more deposition steps, wider tuning range can be obtained. The 3D FDTD simulations (inset of Figure 3(a)) show a linear shift in the resonant wavelength as expected from small perturbations, although there is more uncertainty in the simulations due to the high spatial resolution (\sim a few nanometers or less) required to capture this digital tuning. Figure 3(b) plots the wavelength increment for each deposition step. An average wavelength red shift of 2.443 ± 0.359 nm is obtained for each step, which corresponds to a resonance shift of 122 ± 18 pm per HfO_2 monolayer deposition. An oscillatory variation of the resonance shift is also observed, as shown in Figure 3(b). This is due to variations in the film deposition thickness, which is not perfectly the same in each step. In addition, we observe that the resonance increment itself increases slightly from 2.2 nm to 2.7 nm based on the linear curve fit. This is because, due to the conformality of ALD process, more dielectric material will be added relative to the previous step due to the expanded surface area, so that the resonance increment also slightly goes up, as illustrated in deposition schematics in Figure 1(f).

With different deposition material, the precision of resonant wavelength shift per ALD cycle can be changed. Single monolayer of HfO_2 induces an average 122 pm shift ($n = 1.88$ at $1.55 \mu\text{m}$, 0.93 \AA per ALD cycle at $150 \text{ }^\circ\text{C}$). From first-order perturbation analysis, a monolayer of TiO_2 ($n = 2.18$ at $1.55 \mu\text{m}$, 0.5 \AA per ALD cycle at $100 \text{ }^\circ\text{C}$ [16]) can induce will make 54 pm shift, while a monolayer of Al_2O_3 ($n = 1.57$ at $1.55 \mu\text{m}$, 1 \AA per ALD cycle at $100 \text{ }^\circ\text{C}$ [15]) can generate a 158 pm wavelength shift.

Figure 3(c) illustrates the variation of quality factor Q with the number of deposition steps for all three $L5$ cavities. After first deposition step, Q values drop almost by half for all cavities. We believe this is because the roughness effects of surface and air hole sidewall are magnified initially by the ALD deposited film. During the following deposition steps, the deposited surface is smoother, permitting the Q values to recover back to almost their initial values. The Q values always maintain at least 20,000 or more during the deposition steps, also observed in our 3D FDTD simulations. This demonstrated shift in the resonance, while preserving the cavity Q , in response to a monolayer deposition also suggests these cavities as possible integrated sensors with pronounced responsivity to environmental conditions.

In summary, we have developed a new technique for fine tuning the resonant wavelengths of high- Q/V_m silicon photonic crystal nanocavities digitally using ALD of HfO_2 monolayers. The results demonstrate the total tuning range of around 17 nm limited only by the current number of deposition steps used. The tuning precision is 122 ± 18 pm per ALD cycle while preserving high quality factors of resonant modes in $L5$ photonic crystal nanocavities. With photolithographic lift-off method, dielectric monolayers such as HfO_2 with submicron features can be selectively deposited only at the nanocavity region using low-temperature ALD [24] for even finer tuning control. The highly controlled, digital tuning of high- Q modes in silicon photonic crystal nanocavities allows for practical realization of optical devices involving multiple resonances and matching transitions between quantum dots and optical resonances for cavity quantum electrodynamics.

This work was partially supported by DARPA, the New York State Foundation for Science, Technology and Innovation, and the National Science Foundation (ECS-0622069). The authors acknowledge the support of Mingbin Yu, and Dim-Lee Kwong of the Institute of Microelectronics in Singapore. Xiaodong Yang acknowledges the support of an Intel Fellowship.

References

1. B. S. Song, S. Noda, T. Asano, and Y. Akahane, "Ultra-high-Q photonic double-heterostructure nanocavity," *Nat. Mater.* **4**, 207-210 (2005).

2. E. Kuramochi, M. Notomi, S. Mitsugi, A. Shinya, T. Tanabe, and T. Watanabe, "Ultra-high-Q photonic crystal nanocavities realized by the local width modulation of a line defect," *Appl. Phys. Lett.* **88**, 041112 (2006).
3. P. E. Barclay, K. Srinivasan, and O. Painter, "Nonlinear response of silicon photonic crystal microresonators excited via an integrated waveguide and fiber taper," *Opt. Express* **13**, 801-820 (2005).
4. T. Tanabe, M. Notomi, S. Mitsugi, A. Shinya, and E. Kuramochi, "All-optical switches on a silicon chip realized using photonic crystal nanocavities," *Appl. Phys. Lett.* **87**, 151112 (2005).
5. X. Yang, C. Husko, M. Yu, and D.-L. Kwong, and C. W. Wong, "Observation of femto-joule optical bistability involving Fano resonances in high- Q/V_m silicon photonic crystal nanocavities," submitted to *Appl. Phys. Lett.* (2007); also available at <http://arxiv.org/abs/physics/0703132>.
6. H. Rong, S. Xu, Y. H. Kuo, V. Sih, O. Cohen, O. Raday, and M. Paniccia, "Low-threshold continuous-wave Raman silicon laser," *Nature Photonics* **1**, 232-237 (2007).
7. X. Yang and C. W. Wong, "Coupled-mode theory for stimulated Raman scattering in high- Q/V_m silicon photonic band gap nanocavity lasers," *Opt. Express* **15**, 4763-4780 (2007).
8. R. Bose, X. Yang, R. Chatterjee, J. Gao and C. W. Wong, "Weak coupling interactions of colloidal lead sulphide nanocrystals with silicon photonic crystal nanocavities near 1.55 μm at room temperature," *Appl. Phys. Lett.* **90**, 111117, (2007).
9. E. Peter, P. Senellart, D. Martrou, A. Lemaître, J. Hours, J. M. Gérard, and J. Bloch, "Exciton-Photon Strong-Coupling Regime for a Single Quantum Dot Embedded in a Microcavity," *Phys. Rev. Lett.* **95**, 067401, (2005)
10. C. W. Wong, P. Rakich, S. G. Johnson, M. Qi, H. I. Smith, L. C. Kimerling, E. P. Ippen, Y.-B. Jeon, G. Barbastathis, S.-G. Kim, "Strain-tunable Silicon Photonic Band Gap Microcavities in Optical Waveguides," *Appl. Phys. Lett.* **84**, 1242 (2004).

11. K. Hennessy, A. Badolato, A. Tamboli, P. M. Petroff, E. Hu, M. Atatüre, J. Dreiser, and A. Imamoglu, "Tuning photonic crystal nanocavity modes by wet chemical digital etching," *Appl. Phys. Lett.* **87**, 021108 (2005).
12. S. Mosor, J. Hendrickson, B. C. Richards, J. Sweet, G. Khitrova, H. M. Gibbs, T. Yoshie, A. Scherer, O. B. Shchekin, and D. G. Deppe, "Scanning a photonic crystal slab nanocavity by condensation of xenon," *Appl. Phys. Lett.* **87**, 141105 (2005).
13. S. Strauf, M. T. Rakher, I. Carmeli, K. Hennessy, C. Meier, A. Badolato, M. J. A. DeDood, P. M. Petroff, E. L. Hu, E. G. Gwinn, and D. Bouwmeester, "Frequency control of photonic crystal membrane resonators by monolayer deposition," *Appl. Phys. Lett.* **88**, 043116 (2006).
14. M.F. Al-Kuhaili, "Optical properties of hafnium oxide thin films and their application in energy-efficient windows," *Optical Materials* **27**, 383-387 (2004).
15. T. S. Eriksson, A. Hjortsberg, G. A. Niklasson, and C. G. Granqvist, "Infrared optical properties of evaporated alumina films," *Appl. Opt.* **20**, 2742 (1981).
16. K. Awazu, M. Fujimaki, X. Wang, A. Sai, and Y. Ohki, "Fabrication of two-dimensional photonic structure of titanium dioxide with sub-micrometer resolution by deep x-ray lithography," *Mat. Res. Soc. Symp. Proc.* **820**, R4.5 (2004).
17. J. H. Lee, W. Leung, J. Ahn, T. Lee, I. S. Park, K. Constant, and K. M. Ho, "Layer-by-layer photonic crystal fabricated by low-temperature atomic layer deposition," *Appl. Phys. Lett.* **90**, 151101 (2007).
18. J. Y. Huang, X. D. Wang, and Z. L. Wang, "Controlled replication of butterfly wings for achieving tunable photonic properties," *Nano Lett.* **6**, 2325-2331 (2006).
19. E. Graugnard, D. P. Gaillot, S. N. Dunham, C. W. Neff, T. Yamashita, and C. J. Summers, "Photonic band tuning in two-dimensional photonic crystal slab waveguides by atomic layer deposition," *Appl. Phys. Lett.* **89**, 181108 (2006).
20. A. Deshpande, R. Inman, G. Jursich, and C. Takoudis, "Atomic layer deposition and characterization of hafnium oxide grown on silicon from tetrakis(diethylamino)hafnium and water vapor," *J. Vac. Sci. Technol. A* **22**, 2035-2040 (2004).

21. Ardavan Farjadpour, David Roundy, Alejandro Rodriguez, Mihai Ibanescu, Peter Bermel, J. D. Joannopoulos, Steven G. Johnson, and Geoffrey Burr, "Improving accuracy by subpixel smoothing in FDTD," *Opt. Letters* **31**, 2972–2974 (2006).
22. M. Skorobogatiy, G. Bégin, and A. Talneau, "Statistical analysis of geometrical imperfections from the images of 2D photonic crystals," *Opt. Express* **13**, 2487-2502 (2005).
23. Steven G. Johnson and J. D. Joannopoulos, "Block-iterative frequency-domain methods for Maxwell's equations in a planewave basis," *Opt. Express* **8**, 173-190 (2001).
24. M. J. Biercuk, D. J. Monsma, C. M. Marcus, J. S. Becker, and R. G. Gordon, "Low-temperature atomic-layer-deposition lift-off method for microelectronic and nanoelectronic applications," *Appl. Phys. Lett.* **83**, 2405 (2003).

Figure captions

Fig. 1. (color online) Top-view SEM images of airbridge $L5$ nanocavity with $S_I = 0.02a$ coupled with photonic crystal waveguides before ALD (a) and after 140 ALD cycles of HfO_2 (b). 45°-angle-view SEM images of airbridge photonic crystal slabs before ALD (c) and after 140 ALD cycles of HfO_2 (d). 3D FDTD calculated electric field E_y profile of the high- Q mode supported in $L5$ nanocavities (e). Deposition schematic cross section of the sample morphology (f).

Fig. 2. (color online) (a) Measured cavity resonances after each deposition step (“1” to “7” in legend; “0” is unperturbed) for $L5$ cavity with $S_I = 0.02a$. (b) Magnified resonance peak after the fourth deposition step, quality factor $Q \sim 49,000$.

Fig. 3. (color online) (a) The tuned resonant wavelength scales linearly with the number of deposition step for all three $L5$ cavities under investigation. Inset: 3D FDTD calculated wavelength shift ($\Delta\lambda$) for increasing thicknesses (Δt) of HfO_2 deposited, for all three cavities studied. (b) The wavelength increment ($\delta\lambda$) for each deposition step. (c) The variation of quality factor Q with the number of deposition steps for all three $L5$ cavities.

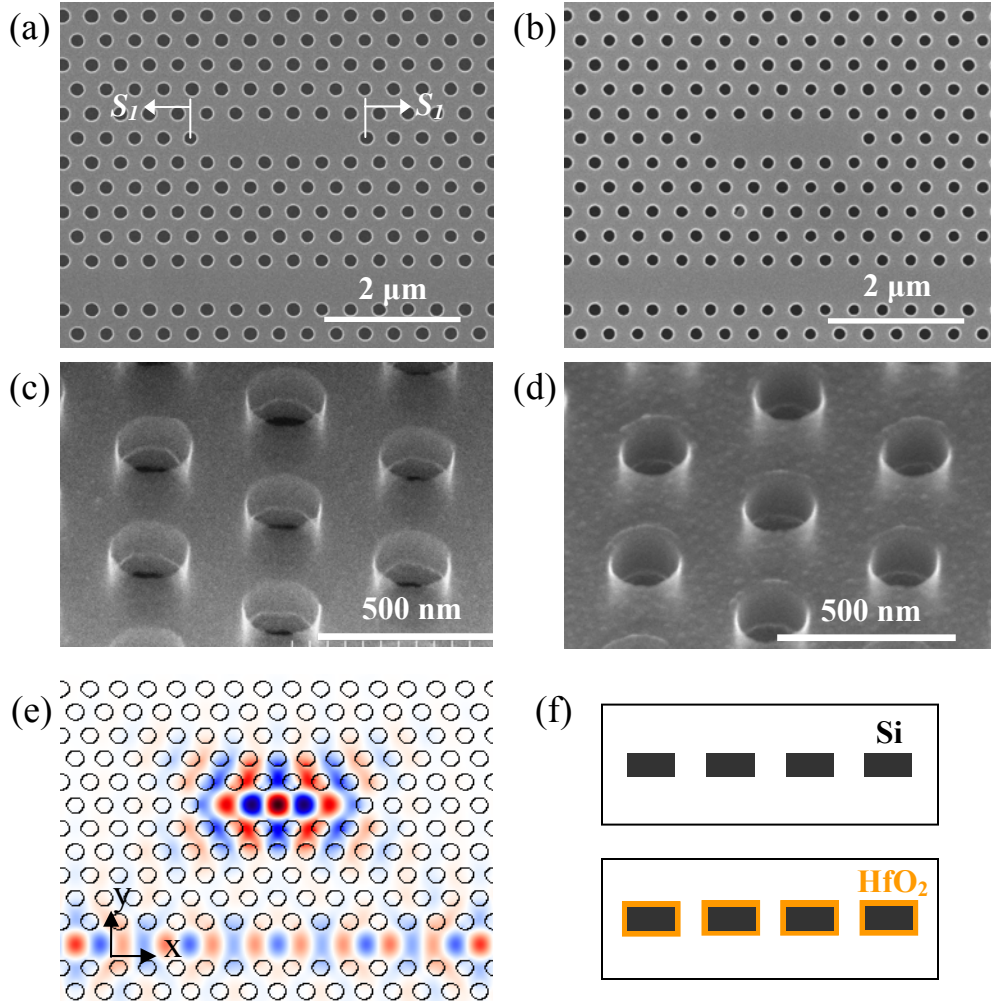


Fig. 1. (color online) Top-view SEM images of airbridge $L5$ nanocavity with $S_1 = 0.02a$ coupled with photonic crystal waveguides before ALD (a) and after 140 ALD cycles of HfO_2 (b). 45°-angle-view SEM images of airbridge photonic crystal slabs before ALD (c) and after 140 ALD cycles of HfO_2 (d). 3D FDTD calculated electric field E_y profile of the high- Q mode supported in $L5$ nanocavities (e). Deposition schematic cross section of the sample morphology (f).

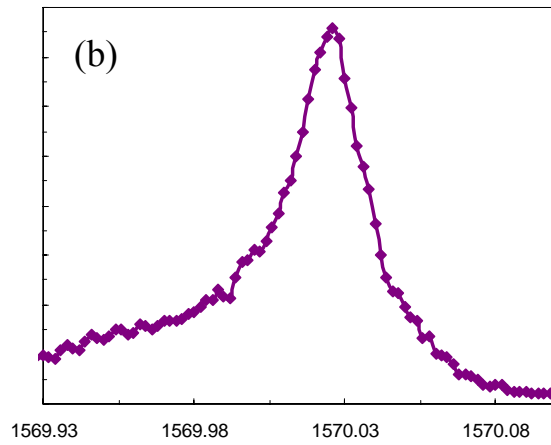
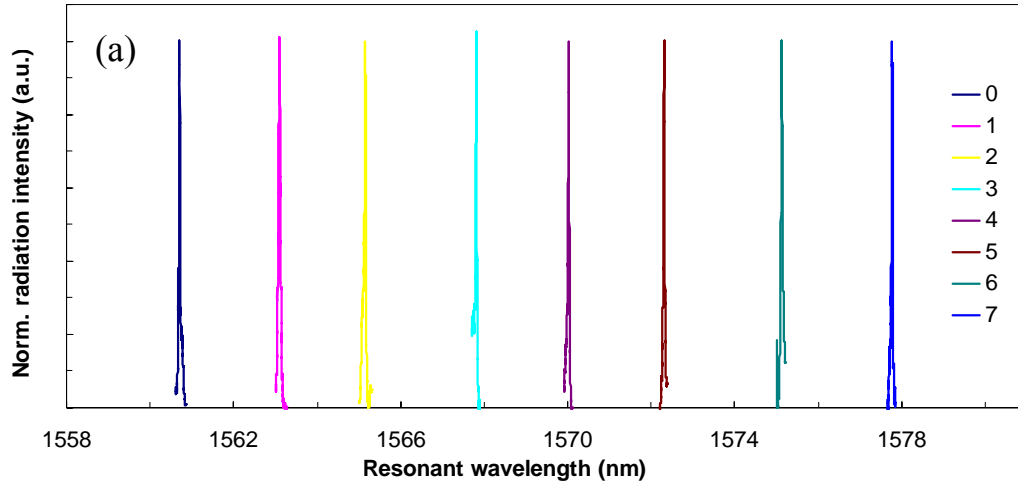


Fig. 2. (color online) (a) Measured cavity resonances after each deposition step (“1” to “7” in legend; “0” is unperturbed) for $L5$ cavity with $S_I = 0.02a$. (b) Magnified resonance peak after the fourth deposition step, quality factor $Q \sim 49,000$.

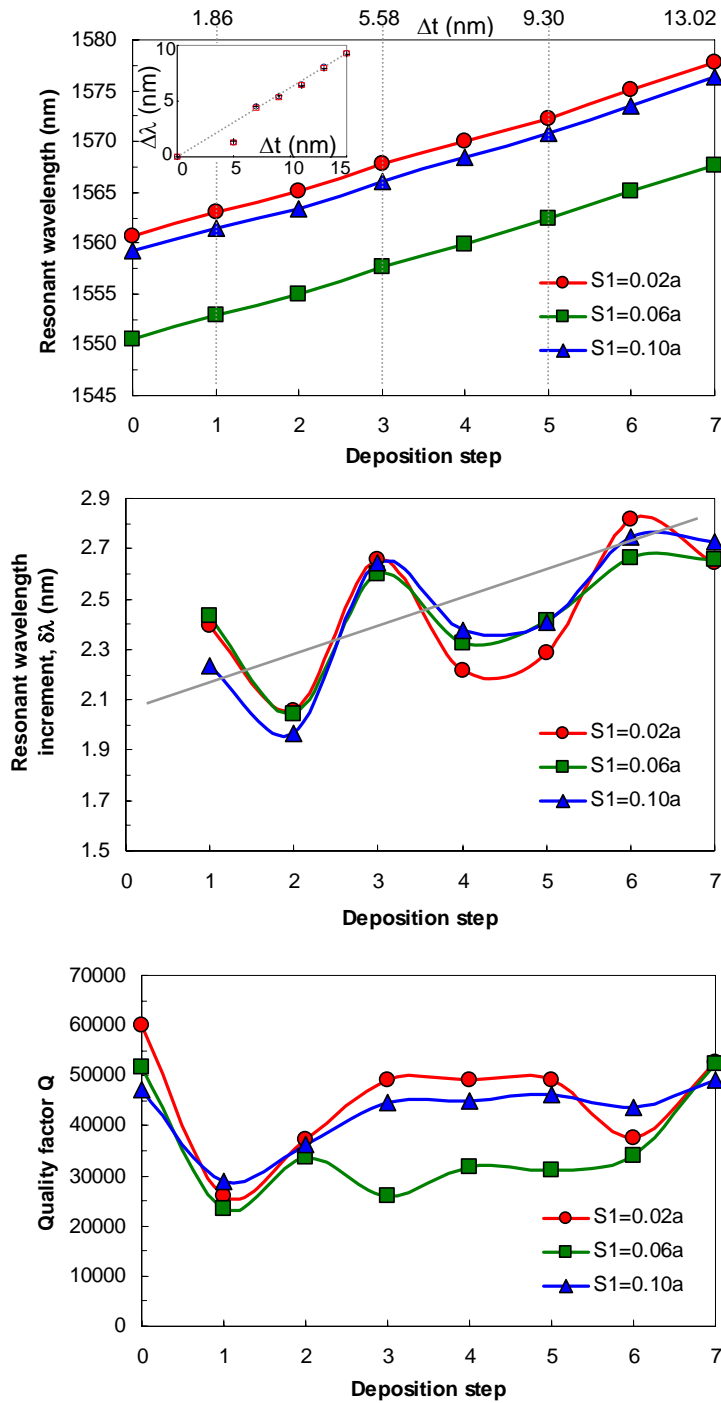


Fig. 3. (color online) (a) The tuned resonant wavelength scales linearly with the number of deposition step for all three $L5$ cavities under investigation. Inset: 3D FDTD calculated wavelength shift ($\Delta\lambda$) for increasing thicknesses (Δt) of HfO_2 deposited, for all three cavities studied. (b) The wavelength increment ($\delta\lambda$) for each deposition step. (c) The variation of quality factor Q with the number of deposition steps for all three $L5$ cavities.